Development of an integrated methodology for the post-flight analysis of the transition payload on the EXPERT mission

By F. Pinna†, K. Bensassi† P. Rambaud†, O. Chazot †, A. Lani AND O. Marxen

Post-flight analysis of the EXPERT mission requires the development of an advance methodology that enables the prediction of transition over hypersonic vehicles. Progress toward this methodology is achieved with the development of a CFD solver and a stability solver. Validation of these tools is achieved by comparison with experimental (VKI) and DNS (CTR) data.

1. Introduction

The EXPERT (European eXPErimental Reentry Testbed) mission started by ESA in 2000 provides a unique opportunity to the European aerospace community for developing scientific payloads and performing in-flight experiments in order to obtain aerothermodynamic data for the validation of numerical models and of ground-to-flight extrapolation methodologies. To this aim, a re-entry vehicle has been designed and equipped with different instrumentations and flight experiments provided by several European research centers and universities. The von Karman Institute (VKI) is currently the primary investigator for two payloads on the EXPERT mission; one provides flight data for gas-surface interaction over TPS junctions, the second provides flight data for roughness induced laminar to turbulent transition. Those payloads, after design and qualification, are currently being integrated on the vehicle. The EXPERT flight is expected in summer 2011. Flight experiments consist of unsteady wall temperature measurements on the vehicle and suitable data-processing will recover the wall heat-flux enabling boundary layer characterization along the EXPERT trajectory. Preparation for post-flight analyses has already started with the development of flight analysis methods and validation strategies. They involve ground testings and advanced CFD capabilities to maximize the benefits of these crucial flight data to the study of aerothermodynamic phenomena and hypersonic vehicle design. This effort is contributing to a renewed interest of the transition community in the study of high-speed flows. Transition prediction is a key element in design of future hypersonic vehicles because high thermal loads associated with turbulent flows have a direct impact on the thermal protection system. Despite many efforts in this field, a unique prediction method is still elusive, and transition itself is proving to be an elusive topic. On the other hand, stability analysis has advanced to the point where it is producing interesting results in prediction of transition. Specially, the e^N method is a cheap, yet scientifically based and effective methodology for design purposes.

A target of the current effort is to present the underlying techniques used in the VKI Expandable Stability and Transition Analysis toolkit (VESTA) that is currently implemented at VKI. Transition and the appearance of turbulence depend strongly on

† von Karman Institute, Aerospace Department

the trajectory of the vehicle so that different points along the trajectory, from high to lower altitude, could correspond to thermo-chemical non-equilibrium, chemical non-equilibrium or equilibrium flows. Each of these regimes should be modeled with its own set of equations. However, the effect of these models on the prediction of the onset of transition is not well appreciated. Malik & Anderson (1991) clearly state that at high altitude and velocities of interest (i.e., in thermo-chemical non-equilibrium) this effect is not necessary a serious issue. Even though a different thermodynamic state alters the growth rate of the perturbations, they argue that transition is more likely to happen at lower altitudes and velocities, where the flow could be treated essentially as a mixture in equilibrium. For these reasons, the present work addresses only LTE flows as a starting block for further improvement.

In hypersonic conditions, the flow is strongly influenced by the behavior of each chemical species. Therefore, the way the reaction rates are computed dramatically changes the resulting solution. The influence of a chemistry model could be higher than the choice of using thermo-chemical non-equilibrium instead of chemical non-equilibrium [see Franko *et al.* (2010)] model representation. The current work is also interesting from this point of view because the transition comparisons with the DNS data of Marxen *et al.* (2010) uses the same chemical library [MUTATION, Magin & Degrez (2004)]. It is expected that a CFD solver should be able to provide laminar profiles at any Mach number at any place around the vehicle to feed the stability methodology. The CFD solver and the stability tool should be integrated in a common methodology in order to have the same treatment of transport properties (e.g., MUTATION). The approach followed in the present effort is first to develop the stability tool to handle natural transition with concurrent developments allowing it to handle isolated roughness, curvature effect, and other difficulties related to real vehicles. The paper first presents the governing equations and the numerical methods used in the CFD solver COOLFLUID with a comparison between VKI-Experimental data the numerical results is given. In the second part of the paper, the stability code is presented, coupling with the CFD solver is discussed, and finally the results are compared with DNS data.

2. CFD

2.1. *Governing equations*

The sets of governing PDEs (Navier-Stokes) describing a two-dimensional flow in a continuum regime can be expressed in conservative and hyper-vectorial form as

$$\frac{\partial \mathbf{U}}{\partial \mathbf{P}} \frac{\partial \mathbf{P}}{\partial t} + \frac{\partial \mathbf{F}_i^c}{\partial x_i} = \frac{\partial \mathbf{F}_i^d}{\partial x_i} + \mathbf{S}; \tag{2.1}$$

where repeated indices imply a sum over x and y, the axial and radial directions respectively, $\mathbf{U}$, the conservative variables, $\mathbf{P}$ the variables used for the solution update, $\mathbf{F}^c$ and $\mathbf{F}^d$, respectively, the convective and diffusive fluxes, and $\mathbf{S}$ is the source term. In the most comprehensive case considered here, namely that of a gas mixture in thermal and chemical non-equilibrium, the conservative and natural variables correspond to a two-temperature model for neutral mixtures Gnoffo *et al.* (2010) can be expressed as follows:

$$\mathbf{U} = (\rho_s, \rho\mathbf{u}, \rho E, \rho e_v)^T, \quad \mathbf{P} = (\rho_s, \mathbf{u}, T, T_v)^T, \tag{2.2}$$

where, in particular, ρ_s represents the partial densities, e_v is the vibrational energy per unit mass, and T_v stands for the vibrational temperature.

2.1.1. *Convective and diffusive fluxes*

The convective and diffusive fluxes are defined by

$$\mathbf{F}^c = \begin{pmatrix} \rho_s \mathbf{u} \\ \rho \mathbf{u}\mathbf{u} + p\hat{I} \\ \rho \mathbf{u} H \\ \rho \mathbf{u} e^v \end{pmatrix}, \ \mathbf{F}^d = \begin{pmatrix} -\rho_s \mathbf{u}_s^d \\ \bar{\bar{\tau}} \\ (\bar{\bar{\tau}} \cdot \mathbf{u})^T - \mathbf{q} \\ -\mathbf{q}_v \end{pmatrix}. \tag{2.3}$$

The tensor of viscous stresses $\bar{\bar{\tau}}$ appearing in Eq. 2.3 is defined as

$$\tau_{ij} = \mu \left[\left(\frac{\partial u_j}{\partial x_i} + \frac{\partial u_i}{\partial x_j} \right) - \frac{2}{3} \nabla \cdot \mathbf{u} \ \delta_{ij} \right] - \delta_{ij} \frac{2}{3} \mu \frac{v}{r} \tag{2.4}$$

and it is computed using Stokes' hypothesis of negligible bulk viscosity effects. Herein, the dynamic viscosity μ is computed rigorously from kinetic theory by using the transport algorithms described in Magin & Degrez (2004).
The mass diffusion fluxes $\rho_s \mathbf{u}_s^d$ are computed by solving the Stefan-Maxwell system of equations which consist of a linear system (in the diffusion fluxes) of as many equations as the chemical species are present in the mixture. The roto-translational and vibrational heat fluxes $\mathbf{q}$ and $\mathbf{q}_v$ are defined as

$$\mathbf{q} = -\lambda \nabla T - \lambda_v \nabla T_v - \sum_s \rho_s \mathbf{u_s} h_s, \quad \mathbf{q}_V = -\lambda_v \nabla T_v - \sum_s \rho_s \mathbf{u_s} h_s^v, \tag{2.5}$$

where the λ is the roto-translational thermal conductivity, λ_v is the vibrational thermal conductivity and the species enthalpies h_s include translational, rotational, vibrational and formation contributions.

2.1.2. *Source terms*

The source terms in Eq. 2.2 can be expressed as

$$\mathbf{S} = \begin{bmatrix} \dot{\omega}_\mathbf{s} & 0 & p & 0 & \dot{\omega}^v \end{bmatrix}^T. \tag{2.6}$$

The mass production/destruction term $\dot{\omega}_s$ for chemical species with partial densities ρ_s which appears in Eq. 2.6 is formulated as follows:

$$\frac{\dot{\omega}_s}{M_s} = \sum_{r=1}^{Nr} \left(\nu_{sr}^{''} - \nu_{sr}^{'} \right) \left\{ k_{fr} \prod_{j=1}^{Ns} \left(\frac{\rho_j}{M_j} \right)^{\nu_{jr}^{'}} - k_{br} \prod_{j=1}^{Ns} \left(\frac{\rho_j}{M_j} \right)^{\nu_{jr}^{''}} \right\}; \tag{2.7}$$

where the forward reaction rates k_{fr} corresponding to a two-species nitrogen mixture.
The term $\dot{\omega}^v$ expresses the energy exchange (relaxation) between vibrational and translational modes and the vibrational energy lost or gained owing to molecular depletion (dissociation) or production (recombination):

$$\dot{\omega}^v = \sum_s \rho_s \frac{(e_{v,s}^* - e_{v,s})}{\tau_s} + \sum_s \tilde{D}_s \dot{\omega}_s; \tag{2.8}$$

where the relaxation time τ_s is given by Millikan & White (1963) with Park's correction for high temperatures Park (1993). .

2.2. *Numerical Method*

2.2.1. *Finite Volume method*

All the results to be presented have been obtained by means of the parallel FV solver for unstructured grids Lani (2009) provided by the COOLFLUID framework. The FV discretization is applied to the system of governing equations written in integral conservation form:

$$\frac{\partial}{\partial t}\int_{\Omega} \mathbf{U}\, d\Omega + \oint_{d\partial\Omega} \mathbf{F}^c \cdot \mathbf{n}\, d\partial\Omega = \oint_{d\partial\Omega} \mathbf{F}^d \cdot \mathbf{n}\, d\partial\Omega + \int_{\Omega} \mathbf{S}\, d\Omega. \tag{2.9}$$

We apply a conventional cell-centered approximation, that assumes solution vectors located at the centroid of each computational cell. Inverse-distance weighted least square reconstruction Barth (1994) is utilized to yield second order accuracy. AUSM$^+$Up scheme has been utilized for discretizing the convective fluxes

2.2.2. *Implicit Time integration*

The choice of a linear Backward Euler for driving the solution to steady state leads to rewriting the system eq. (2.9) as follows:

$$\frac{\mathbf{U}(\mathbf{P}) - \mathbf{U}(\mathbf{P}^n)}{\Delta t} + \mathbf{R}^{FV}(\mathbf{P}) = 0 = \tilde{\mathbf{R}}(\mathbf{P}); \tag{2.10}$$

where $\tilde{\mathbf{R}}(\mathbf{P})$ is a pseudo-steady residual, $\mathbf{U} = \mathbf{U}(\mathbf{P})$ an explicit analytical relation, and $\mathbf{P}$ the vector of natural variables (defined in eq. 2.2) in which the governing equations are explicitly closed and in which it is therefore convenient to store the solution vector. The application of a one step Newton method yields the following linear system:

$$\left[\frac{\partial \tilde{\mathbf{R}}}{\partial P}(\mathbf{P}^n)\right] \Delta \mathbf{P}^n = -\tilde{\mathbf{R}}(\mathbf{P}^n), \tag{2.11}$$

where the jacobian matrix $\frac{\partial \tilde{\mathbf{R}}}{\partial \mathbf{P}}$ is computed numerically with respect to the natural variables and assuming a first order stencil. The GMRES algorithm with an Additive Schwartz preconditioner provided by the PETSC library serves to solve in parallel the corresponding linear systems arising from Newton linearizations. The solution update is also performed in natural variables.

2.3. *Results*

Numerical simulations of hypersonic flow over a flat plate with a 0.5[mm] leading edge have been done. Two different free stream conditions have been considered and correspond to the free-stream conditions in VKI-H3 (M=6, P = 490 [Pa] and T= 50 [K]) and VKI-Longshot (M=14, P = 137 [Pa] and T= 41 [K]) hypersonic wind tunnels. In both cases the gas is considered calorically perfect and no dissociation is considered. Figure 1a shows the heat flux profile along the flat plate for H3 conditions and 1b shows the heat flux profile along the flat plate and comparison with experimental data obtained in the VKI-Longshot wind tunnel.

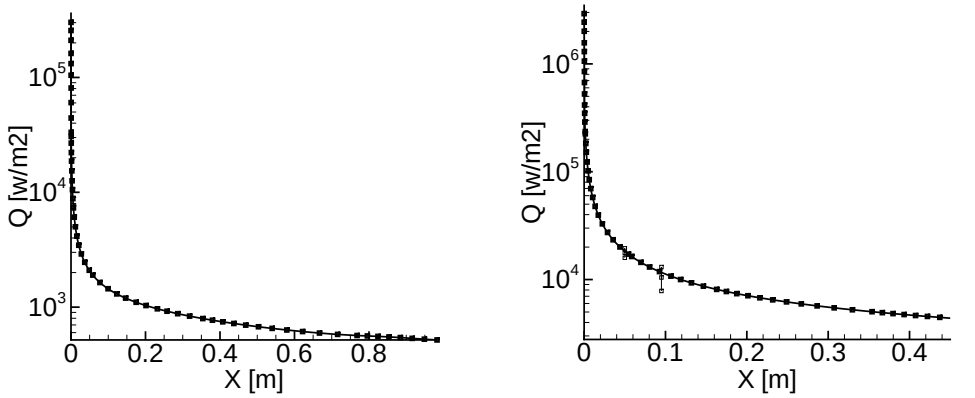

(a) VKI-H3 conditions : M_∞=6 (b) VKI-Longshot conditions : M_∞=14

Figure 1: Heat flux profile along the flat plate: solid line represents laminar CFD, squares are the experimental data

3. Linear stability

Linear stability equations for LTE flows are retrieved by using the linear stability theory (LST) hypotheses: the instantaneous flow is taken as a sum of a mean flow and a perturbation

$$Q(x,y,z,t) = \overline{Q}(x,y,z) + q'(x,y,z,t); \tag{3.1}$$

where q' represents a generic variable disturbance. Eq. (3.1) is substituted in eq. (2.1) and linearized around the mean flow. This decomposition is applied also to the transport and thermodynamic properties, which for our case leads to expression similar to the following one:

$$\mu' = \frac{\mathrm{d}\mu}{\mathrm{d}T}T' + \frac{\mathrm{d}\mu}{\mathrm{d}p}p'. \tag{3.2}$$

Another key hypothesis in LST assumes that each perturbation propagates independently. These are called modes and for a general disturbance are represented by:

$$q'(x,y,z,t) = \tilde{q} \cdot \exp(i\alpha x + i\beta z - i\omega t) + c.c.\ ; \tag{3.3}$$

where the $\tilde{q}$ term is the amplitude function, α and β are the stream-wise and span-wise wavenumber, and ω is the frequency
An air-5 mixture (N_2,O_2,N,O,NO) is used in the present work to compute the rates and the flow properties, and the gas state equation is re-written as

$$p = \rho r T \zeta; \tag{3.4}$$

where r is the gas constant for the undissociated gas N_2-O_2 mixture and $\zeta = M_{und}/M_{dis}$ is the so called compressibility factor.
Navier-Stokes equations have been non-dimensionalized using reference quantities: length is scaled by $l = \sqrt{\nu_e x_e/U_e}$, velocity by U_e, density by ρ_e, pressure by $\rho_e U_e^2$, time by l/U_e, and temperature by T_e. The reference viscosity (both first and second coefficient) is , for sake of consistency, the value corresponding to T_e and p_e.

The set of equations reads as

continuity equation

$$HP\left(-\frac{T_y\zeta_T}{\zeta}-\frac{T_y}{T}\right)\tilde{v}+FH\Psi\tilde{p}+GH\frac{P}{T}\Psi\tilde{T}+i\beta HP\tilde{w}+HP\tilde{v}_y+i\alpha HP\tilde{u}=0 \quad (3.5)$$

x momentum equation

$$\begin{aligned}&\frac{HP}{T\zeta}\left(\Psi\tilde{u}+U_y\tilde{v}\right)=\frac{1}{Re}\left(\mu_P U_{yy}+\mu_{PT}T_yU_y-i\alpha\right)\tilde{p}+\frac{1}{Re}\left(\mu_T U_{yy}+\mu_{TT}T_yU_y\right)\tilde{T}+\\&+\frac{1}{Re}\left[\mu_p U_y\tilde{p_y}+\mu_T U_y\tilde{T_y}+\left(i\alpha\mu_T T_y\right)\tilde{v}+\mu_T T_y\tilde{u}_y+i\alpha\left(\mu+\lambda\right)\tilde{v}_y\right]+\\&-\frac{1}{Re}\left[\alpha\beta\left(\mu+\lambda\right)\tilde{w}+u_{yy}\mu-\left(\alpha^2\left(\lambda+2\mu\right)+\mu\beta^2\right)\tilde{u}\right]\end{aligned} \quad (3.6)$$

y momentum equation

$$\begin{aligned}&\frac{HP}{T\zeta}\Psi\tilde{v}=\frac{1}{Re}\left[\left(i\beta\mu_P W_y+i\alpha\mu_P U_y\right)\tilde{p}+\left(i\beta\mu_T W_y+i\alpha\mu_T U_y\right)\tilde{T}\right]+\\&\frac{1}{Re}\left[\left(2\mu_T+\lambda_T\right)T_y\tilde{v}_y+i\beta\lambda_T T_y\tilde{w}+i\alpha\lambda_T T_y\tilde{u}+i\beta\left(\mu+\lambda\right)\tilde{w}_y\right]-\tilde{p}_y+\\&\frac{1}{Re}\left[(2\mu+\lambda)\tilde{v}_y y-\mu\left(\beta^2+\alpha^2\right)+i\alpha\left(\mu+\lambda\right)\tilde{u}_y\right]\end{aligned} \quad (3.7)$$

z momentum equation

$$\begin{aligned}&\frac{HP}{T\zeta}\left(\Psi\tilde{w}+W_y\tilde{v}\right)=\frac{1}{Re}\left[\left(\mu_P W_{yy}\mu_{PT}T_yW_y\right)\tilde{p}+\left(\mu_T W_{yy}+\mu_T T T_y W_y\right)\tilde{T}+\mu_p W_y\tilde{p_y}\right]+\\&+\frac{1}{Re}\left[\mu_T W_y\tilde{T_y}+\mu_T T_y\tilde{w}_y+i\beta\mu_T T_y+\mu\tilde{w}_{yy}\right]-i\beta\tilde{p}+\\&-\frac{1}{Re}\left[\left(\beta^2(2\mu+\lambda)+\alpha^2\mu\right)\tilde{w}+i\beta\mu\tilde{v}_y-\alpha\beta\mu\tilde{u}+i\beta\lambda\tilde{v}_y-\alpha\beta\lambda\tilde{u}\right]\end{aligned} \quad (3.8)$$

energy equation

$$\begin{aligned}&\frac{HP}{T\zeta}\left[\left(h_T\Psi\tilde{T}+h_P\Psi\tilde{p}\right)+h_T T_y\tilde{v}\right]=\frac{1}{PrRe}\left[\left(2k_T T_y\right)\tilde{T}_y+k_P T_y\tilde{p}_y+k\tilde{T}_{yy}\right]\\&\frac{Ec}{Re}\left(\left(W_y^2+U_y^2\right)\left(\mu_P\tilde{p}+\mu_T\tilde{T}\right)+i2\mu\left(\beta W_y+\alpha U_y\right)\tilde{v}+2\mu W_y\tilde{w}_y+2\mu U_y\tilde{u}_y\right)+\\&+Ec\Psi\tilde{p}+\frac{1}{PrRe}\left[\left(k_T T_{yy}^2+k_{TT}T_y^2-\left(\alpha^2+\beta^2\right)k\right)\tilde{T}+\left(k_P T_{yy}+k_{PT}T_y^2\right)\tilde{p}\right]\end{aligned} \quad (3.9)$$

where $\Psi = i\alpha U + i\beta W - i\omega$, $F = 1 - \left.\frac{\partial \ln\zeta}{\partial p}\right|_T$, $G = 1 + \left.\frac{\partial \ln\zeta}{\partial T}\right|_p$ and $H = c_p\, Ec/r$. This set of equations could be reduced to a system in the form

$$\left[AD^2+BD+C\right]\chi=0 \quad (3.10)$$

being $\chi = [\tilde{u}, \tilde{v}, \tilde{p}, \tilde{T}, \tilde{w}]$ and $D = \mathrm{d}/\,\mathrm{d}y$ the derivative operator.

3.1. *thermodynamic and transport properties*

Without the thermodynamic and transport properties values it is impossible to solve the stability equations. For this purpose the MUTATION library has been used and further details could be found in Magin & Degrez (2004). This library has a front-end (called MUTATION code) that could be used to run interactively or inside a shell script. Although a call to the MUTATION library could be performed directly by the stability

software this approach is somehow more expensive as every derivative require multiple computations for a single (p, T) pair.
Partial derivatives with respect to temperature and/or pressure are obtained by computing first the selected property on a range of p and T spaced according to Chebyshev point spacings

$$y = \cos(\frac{\pi(2j+1)}{2(N+1)}); \tag{3.11}$$

where N is the total number of points, and in a second step by deriving the interpolants

$$u(x)'_{interp} = \sum_{n=0}^{N-1} a_n^{(1)} T_n(x) \tag{3.12}$$

where

$$a_n^{(1)} = \frac{2}{c_n} \sum_{\substack{p=n+1 \\ p+n \text{ odd}}}^{N} p a_p \quad \text{where} \qquad c_n = \begin{cases} 2 & n = 0 \\ 1 & n > 0 \end{cases}. \tag{3.13}$$

3.2. *Numerical Method*

Stability of compressible flows in chemical equilibrium has been studied by means of Chebyshev collocation method. This method is flexible and accurate [see Canuto *et al.* (1987)]. A set of Gauss-Chebyshev-Lobatto points has been chosen

$$x_j = \cos\left(\frac{j\pi}{N}\right). \tag{3.14}$$

Given a function v defined on the afore mentioned points, it is possible to obtain its derivative by defining a polynomial p that satisfy the usual condition for an interpolation problem $p(x_j) = v_j$ for $j = 0, \ldots, N$ and then computing its derivative $w_j = p'(x_j)$.This is a linear operation and it could be represented as a simple multiplication by an $(N + 1) \times (N+1)$ matrix $w = D_N \cdot v$. Note that m-th order derivative could be easily computed by $(D_N)^m$.

The algebraic mapping proposed in Malik (1990) has been used to transform Chebyshev polynomials defined in $x = [-1, 1]$ to the physical domain $y = [0, \infty)$ (truncated arbitrarily in $y = [0, y_{max}]$)

$$y = a\frac{1+x}{b-x}; \tag{3.15}$$

where $b = 1+2a/y_{max}$ and $a = y_i y_{max}/(y_{max}-2y_i)$ with y_i corresponding to the location $x = 0$.

3.3. *Boundary conditions*

There are four homogeneous boundary condition for $\tilde{u}$, $\tilde{v}$, $\tilde{w}$, $\tilde{T}$. These homogeneous Dirichlet b.c. can be easily plugged into the collocation method by skipping the first and the last rows and columns [D_N becomes a $(N-1) \times (N-1)$ matrix]. Two zeros at the extremities of the resulting w could be appended so that the final vector has the correct dimension. In case of a Neumann boundary conditions the problem could be overcome by extracting the corresponding row from the matrix D_1. As nothing is prescribed on pressure, one could either use a staggered grid as in Khorrami *et al.* (1989) or introduce a somehow fictitious boundary condition on pressure. This could be achieved by re-writing

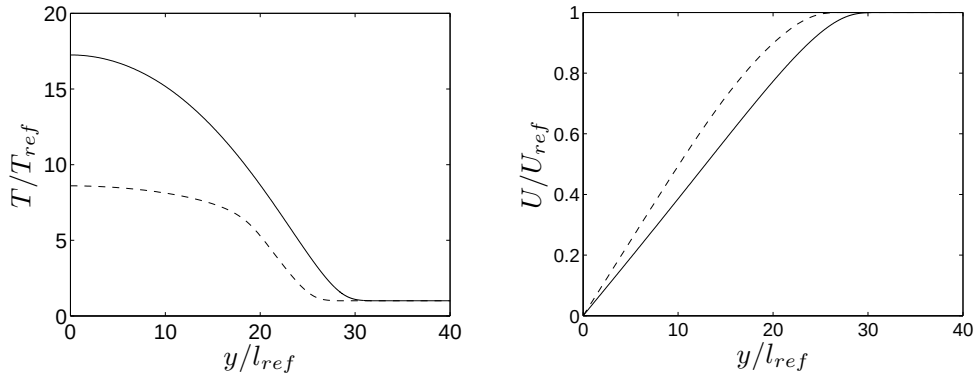

(a) non-dimensional temperature profile (b) non-dimensional velocity profile

Figure 2: non-dimensional profiles for Mach 10 flow at $Re_l = 2000$: ····· LTE, —— CPG

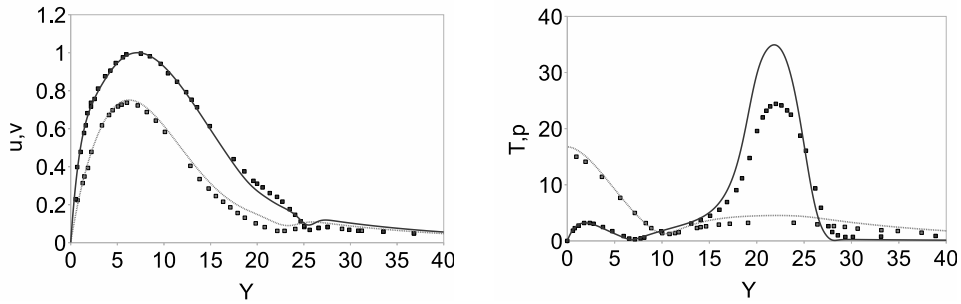

(a) stream wise and wall normal velocity (b) temperature and pressure

Figure 3: perturbation profile referred to the most unstable mode for a Mach 10 flow at $Re_l = 2000$ and $\omega = 0.068$: ■ DNS, —— LST

the y-momentum equation at the boundaries and adding them to the system eq.(3.10) as new equations to be solved:

$$\left.\frac{\partial \hat{p}}{\partial y}\right|_{y=0,y_{max}} = X_{0,m}. \tag{3.16}$$

The variable vector gains two more variables, namely $\tilde{p}_0$ and $\tilde{p}_N$, and two new equations are introduced by appending two rows and two columns to the matrices reaching a final dimension of $(5N-3)$.

3.4. *Stability of a compressible flows on a flat plate at Mach 10*

The case proposed in Malik & Anderson (1991), and also analyzed in Marxen *et al.* (2010), has been computed. The flow has an adiabatic wall with $Pr_\infty = 0.69$ with $Re_{c_\infty} = \frac{\rho_\infty c_\infty L_{ref}}{\mu_\infty} = 10^4$, $T_\infty = 350K$, $p_\infty = 3596Pa$. The mean velocity and temperature profiles have been provided by Marxen, who used the same library MUTATION to compute the transport properties and enthalpy. This is a particularly interesting case as chemistry strongly affects the final results and comparison between groups is not always

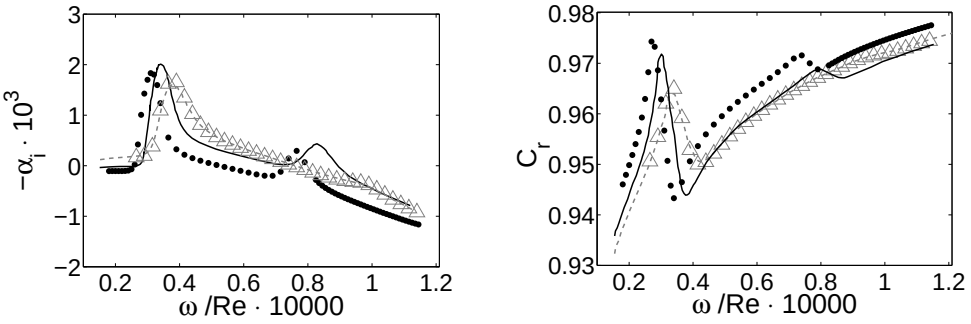

(a) growth rate

(b) phase velocity

Figure 4: $Re_l = 2000$, $\omega = 0.068$, $\beta = 0$, Mach 10, comparison with Malik's computation: present LTE •, Malik's LTE ——— , present CPG △, Malik's CPG – – – –

straightforward owing to the differences that various researchers use to compute the transport and thermodynamic properties. Thus this work presents a direct comparison of DNS and LST. Figure 2 shows profile comparison between calorically perfect gas and LTE at the same condition. We first should note that the velocity profile is less affected than the temperature profile. The value of the temperature at the wall is half of the value obtained with calorically perfect gas. This is completely understandable as the specific heat constant increases with temperature. In addition, the boundary layer height is somewhat smaller. These differences are reflected in the shape of the most unstable eigenfunctions showing that the peaks and all other features of the perturbation profiles are shifted toward the wall for the LTE computation.
Figure 3 shows profiles from DNS and LST for velocity, temperature and pressure of the most unstable mode. A good match is obtained between the two methods for pressure and velocity. Temperature, on the other hand, shows some differences though the overall agreement is satisfactory at the moment.
Some interesting information is also coming from the plot of the phase velocity and growth rate for the same fixed ω but with varying Reynolds numbers. Results are compared against the ones presented by Malik. It is evident that the introduction of chemistry produces a second peak in the growth rate graph as shown in Fig. 4a. This is the third mode that is not visible in the calorically perfect gas computations. Another point to note is that, though the present CPG computation agrees perfectly with Malik's results, the present LTE computation is somehow shifted toward lower frequencies for the same growth rate. A similar behavior is also found in the phase velocity plot.

4. Conclusions

In this short paper, methodology leading to the prediction of natural transition in hypersonic flow regime is proposed. A laminar version of the VKI COOLFLUID code is presented, and its results are briefly compared with the experimental database obtained at VKI during the preparation of the EXPERT mission. An interpolation method for the gas properties of the flow has been proposed allowing a faster computation thus optimizing the access to the external MUTATION chemistry library. The CFD solver is ready to provide profiles to be analyzed with the VKI stability set of solvers, VESTA. A solu-

tion from VESTA is presented and compared with a case previously reported in Marxen *et al.* (2010) and Malik & Anderson (1991). Good agreement is found between DNS and linear stability theory for the most unstable eigenvalue when the same chemistry library is used for the thermodynamic and transport properties. Comparison with the original computation of Malik & Anderson (1991) shows perfect agreement for the growth rate for calorically perfect gas. The LTE growth rate graph results in a plot similar to what was proposed by Malik, although slightly shifted to lower frequencies.

5. Acknowledgments

The financial participation provided by the FNRS to attend the CTR Summer Program is acknowledged as well as the invaluable help of Thierry Magin, Nagi Mansour and Davide Masutti for their constant support and motivation before, during, and after the summer program.

REFERENCES

Malik, M. R. & Anderson, E. C. 1991 Real gas effects on hypersonic boundary-layer instabilities. *Phys. Fluids A* **3** (5) 803–820.

Marxen, O. J., Magin, T., Iccarino, G., & Shaqfeh, E. S. G. 2010 Hypersonic boundary-layer instability with chemical reactions. *AIAA Paper* 2010-707.

Canuto, C., Hussaini, M. Y., Quarteroni A., Zang T. A. 1988 *Spectral Methods in Fluid Dynamics*, Springer-Verlag.

Boyd, J. P. 2001 *Chebyshev and Fourier spectral methods* Dover.

Khorrami, M. R., Malik, M. R., & Ash, R. L. 1989 Application of spectral collocation techniques to the stability of swirling flows. *J. Comput. Phys.*, 81:206–229.

Malik, M. R. 1990 Numerical methods for hypersonic boundary layer stability. *J. Comput. Phys.*, 86(2):376–413.

Franko, K. J., MacCormack R. W., Lele S. K. 2010 Effects of chemistry modeling on hypersonic boundary layer linear stability prediction. *40th Fluid Dynamics Conference and Exhibit*, AIAA 2010-4601.

Johnson, H. B., Candler G. V. 2010 Orbiter boundary layer stability analysis at Flight entry condition *48th AIIA Aerospace Sceinces Meeting*, AIAA 2010-457.

Magin, T. & Degrez, G. 2004 Transport algorithms for partially ionized and unmagnetized plasmas. *J. Comput. Phys.*(198) 424.

Millikan, R. C. & White, D. R. 1963 Systematics of vibrational relaxation. *J. of Chem. Phys.* 39(12):3209-3213

Park, C. 1993 Review of chemical-kinetic problems of future NASA mission, II: Mars Entries. *J. of Thermophys. and Heat Transfer* (7):385-398

Lani, A. 2009 An object oriented and high performance platform for aerothermodynamics simulation. *Phd Thesis,Von Karman Institute for Fluid Dynamics*.

Barth, T. 1994 Aspects of unstructured grids and finite volume solvers for the Euler and Navier-Stokes equations. *25th Computational Fluid Dynamics Lecture Series*.

Gnoffo, P. A., Gupta, R. N. & Shinn, J. L. 1989 Conservation equations and physical models for hypersonic air flows in thermal and chemical non-equilibrium. *NASA Technical Paper* 1989-2867.